Supporting Information

for

Mode selectivity in methane dissociative chemisorption on Ni(111)

Bin Jiang,[1,a] Rui Liu,[2,a] Jun Li,[1] Daiqian Xie,[3,b] Minghui Yang,[2,b] and Hua Guo [1,b]

[1]*Department of Chemistry and Chemical Biology, University of New Mexico,*

Albuquerque, New Mexico, 87131

[2] *Key Laboratory of Magnetic Resonance in Biological Systems, State Key Laboratory of Magnetic Resonance and Atomic and Molecular Physics, Wuhan Centre for Magnetic Resonance, Wuhan Institute of Physics and Mathematics, Chinese Academy of Sciences, Wuhan 430071, P. R. China*

[3]*Institute of Theoretical and Computational Chemistry, Key Laboratory of Mesoscopic Chemistry, School of Chemistry and Chemical Engineering, Nanjing University, Nanjing 210093, China*

[a]*: equal contributions*

[b]*: corresponding authors*

S-I. Methods and computational details

A. Site and lattice effects

The reaction probabilities obtained in our eight-dimensional (8D) dynamical model ignore the different sites on the Ni(111) surface that have higher barriers. If we only consider the molecule at normal incidence to the surface and the collision time is short, the site effect along the lateral coordinates (*X*, *Y*) can be included within a simple sudden approximation. Following Jackson and Nave,[1] the barrier corrugation is approximately described as follows:

$$\Delta V(X,Y)=\frac{1}{2}M_{CH_4}\left\{\omega_x^2[X-X_{TS}]^2+\omega_y^2[Y-Y_{TS}]^2\right\}, \tag{1}$$

where X_{TS} and Y_{TS} are the lateral coordinates of the saddle point, M_{CH_4} is the CH_4 mass, and ΔV is the difference between the barriers are (*X*, *Y*) and (X_{TS}, Y_{TS}). The harmonic frequencies for lateral motion at the transition state, ω_x and ω_y, are calculated to be 133 and 120 cm^{-1} respectively, which are close to the values reported in previous work.[2-3] A further assumption is made that reaction probabilities at different impact sites have the same shape and only depend on the barrier height. Consequently, the probability for a specific (*X*, *Y*) site is obtained by shifting the ΔV =0 probability:[1]

$$\Theta(E_Z;X,Y)\approx\Theta_0[E_Z-\Delta V(X,Y);X_{TS},Y_{TS}], \tag{2}$$

where Θ_0 is the probability obtained by quantum wavepacket calculations on our potential, namely (*X*, *Y*)= (X_{TS}, Y_{TS}), Θ is thus the probability at a different site (*X*, *Y*), and $\Delta V(X,Y)$ is the barrier shift. We then average over the results for many (*X*, *Y*) sites which cover the surface unit cell, sampling all possible impact sites on the surface. The consequence of the site-averaging is an increased effective barrier and shift of the probability curve towards a higher energy. This site-averaging model has been shown to work well for the dissociative chemisorption of H_2 on the Cu(111) surface[4] and that of CH_4 on the Ni(100) surface.[1]

The two other important effects ignored in our dynamical model relate to the motion of surface atoms. First, it is well known that the Ni atom at the adsorption site puckers near the transition state, which lowers the barrier.[5-9] This so called "electronic coupling" can be reasonably described by a potential term $-\beta Q$,[1,3] where *Q* is the displacement of the Ni atom from the surface plane. In addition, the vibration of the surface atom also influences the location of the transition state alone the *Z* axis. This so-called "mechanical coupling" can be described by a displacement αQ.[1,3,10] The values of the parameters α and β are taken from previous calculations of Tiwari *et al.* ($\alpha = 0.70$, $\beta = 1.16$ eV/Å).[10] It has been shown by Jackson and coworkers[1,9-10] that the electronic coupling can be reasonably approximated within a sudden approximation due to the large mass of the Ni atom, while the mechanical coupling can be treated using a surface mass model.[10-11]

Specifically, we first model the mechanical coupling by substituting the collision coordinate *Z* with $Z' = Z - \alpha Q$ and the corresponding mass M_{CH_4} in Eq. (2) of the main text with $\mu_T = M_s' M_{CH_4}/(M_s' + M_{CH_4})$, where $M_s' = M_s/\alpha^2$ and M_s is the mass of the Ni atom. The reaction probability is then computed with the mass-modified Hamiltonian with Q=0. The resulting single-site reaction probability in the center of mass (COM) energy $\Theta^{Q=0}_{\text{single-site}}(E_{com})$ is then averaged over all possible (X, Y) sites to yield the site-averaged reaction probability $\Theta^{Q=0}_{\text{site-averaged}}(E_{com})$, using the method discussed above. The site averaging is followed by the correction of the electronic coupling, which is approximated by a Boltzmann sampling of Q using an E-shifting scheme, in which the probability for $Q \neq 0$ is obtained by a shift with an amount of barrier difference with Q=0 (namely $-\beta Q$). Finally, this probability $\Theta^{Q-\text{averaged}}_{\text{site-averaged}}(E_{com})$ can be averaged over the lattice atom momentum P to include the mechanical coupling and provide the final temperature dependent initial sticking probability $S_0(E_Z, T)$ as function of normal incident energy (E_Z). In practice, the integral averaged over P can be converted to one over E_{com} as,[10]

$$S_0(E_Z, T) = \int dE_{com} \sqrt{\frac{M_s{}'}{4\pi T \mu_T E_{com}}}\, e^{-\frac{M_s{}'}{2k_B T}\left(\sqrt{\frac{2E_{com}}{\mu_T}} - \sqrt{\frac{2E_Z}{M}}\right)^2} \Theta^{Q-\text{averaged}}_{\text{site-averaged}}(E_{com}) \,. \tag{3}$$

Here, T is the surface temperature and k_B is Boltzmann constant. E_{com} is related to the lattice atom momentum (P) as follows

$$E_{com} = \frac{1}{2}\mu_T \left(\sqrt{\frac{2E_Z}{M_{\text{CH}_4}}} - \alpha \frac{P}{M_s}\right)^2 , \tag{4}$$

where the term in parenthesis is the relative methane-lattice atom collision velocity for a given incident energy E_Z and lattice atom momentum P.

B. Reaction path Hamiltonian

To better understand the mode selectivity in the dissociative chemisorption of CH_4 on Ni(111), we have analyzed the reaction path Hamiltonian[12] on the DFT-based PES. Using POLYRATE 9.7,[13] the minimum energy path (MEP) was determined using Page and McIver's method,[14] starting from the saddle point geometry and going downhill to both directions towards the reactants and products in mass-weighted Cartesian coordinates with step size of 0.00378 $amu^{1/2}$•bohr. The Hessian matrix was calculated at every point along this reaction path. Along the MEP, the reaction coordinate, s, is defined as the signed distance from the saddle point (s=0), with s>0 referring to the product side and s<0 to the reactant side. All calculations are carried out in mass-scaled coordinates with a reduced mass μ equal to 1 amu. The reaction path were followed between s = -9.45 (reactant side) and 3.78 (product side) $amu^{1/2}$•bohr. Since the PES is less reliable in the product channel due to the limitations of our model, only the region immediately after the transition state was included in the analysis. These parameters have been tested for convergence.

A generalized normal-mode analysis was then performed along the MEP using the redundant internal coordinate method.[15-16] With the frequencies of these modes along the reaction coordinate, the vibrationally adiabatic potentials can be obtained

$$V_a(\nu,s) = V_{MEP}(s) + \varepsilon_{\text{int}}(\nu,s)\,, \tag{5}$$

where $V_{MEP}(s)$ is the classical MEP potential and $\varepsilon_{\text{int}}(\nu,s)$ is the vibrational energy at s. The couplings between the mth normal mode and the reaction coordinate (F),

$B_{mF}(s)$,[12] were also calculated. These couplings $B_{mF}(s)$ are the components of the reaction path curvature, κ(s), defined as

$$\kappa(s) = \left(\sum_{m=1}^{F-1} [B_{mF}(s)]^2 \right)^{1/2} \tag{6}$$

and they control the non-adiabatic flow of energy between these modes and the reaction coordinate. They also allow us to give some qualitative explanations of the effects of reactant vibrational excitation on reactivity.

The non-adiabatic couplings between different adiabatic vibrational states can be characterized by the so called “Massey velocity” (v_m) and “Massey parameter” (M_p).[17] The former can be evaluated along the reaction coordinate s,

$$v_m = \frac{\left| \varepsilon_a^i - \varepsilon_b^i \right|}{\left| \hbar \left\langle \psi_a^i \left| \frac{\partial}{\partial s} \right| \psi_a^i \right\rangle \right|}, \tag{7}$$

where ε_a^i and ε_b^i are the ath and bth vibrational eigenvalues at the ith point along the reaction coordinate, ψ_a^i and ψ_b^i are associated vibrational wavefunctions. As suggested by Krishnamohan *et al.*,[2] the vibrational wave functions can be approximated using the normal mode eigenvectors, χ_a^i and χ_b^i, and the partial differential expression in the denominator can be calculated using a finite differencing method,

$$\left\langle \psi_a^i \left| \frac{\partial}{\partial s} \right| \psi_a^i \right\rangle = \frac{\left\langle \chi_a^i \middle| \left(\left| \chi_a^{i+1} \right\rangle - \left| \chi_b^{i-1} \right\rangle \right) \right.}{s_{i+1} - s_{i-1}}. \tag{8}$$

The Massey velocity is then determined by,

$$v_m = \frac{\left|\varepsilon_a^i - \varepsilon_b^i\right|}{\left|\hbar \frac{\left\langle \chi_a^i \middle| \chi_a^{i+1} \right\rangle - \left\langle \chi_a^i \middle| \chi_b^{i-1} \right\rangle}{s_{i+1} - s_{i-1}}\right|} . \tag{9}$$

The influence of the non-adiabatic couplings depends on the relative magnitude between the Massey velocity and the velocity of the colliding molecules along the reaction coordinate (v_s), which defines the Massey parameter,

$$M_\mathrm{p} = v_m / v_s . \tag{10}$$

If v_s is much smaller than v_m, the molecule tends to stay on the adiabatic curve. On the other hand, the molecule in a vibrational state tends to move to the other vibrational adiabatic curve *via* non-adiabatic coupling, if v_s is much larger than v_m. Here, v_s is derived from the kinetic energy along the reaction coordinate (T_s) at the avoid crossing region,

$$v_s = \sqrt{2T_s} , \tag{11}$$

where T_s is estimated by subtracting the potential energy at the avoid crossing region (V_{ac}) and adding the vibrational energy loss (ΔE_{vib}) from initial kinetic energy (T_i),

$$T_s = T_i + \Delta E_{vib} - V_{ac} . \tag{12}$$

It should be noted that the mass-scaled reaction coordinates are used in our reaction path analysis, the resulting v_m and v_s are also mass-scaled velocities.

F. Sudden Vector Projection Model

The adiabatic model assumes the system follows the MEP with an infinitesimal collision velocity. Although non-adiabatic transitions can be introduced to describe collision events with finite translational energy, it might not be an ideal paradigm for considering mode selectivity, particularly for reactions with late barriers. Here, we propose a sudden model, which assumes the collision is an instantaneous event in which the intramolecular vibrational redistribution (IVR) does not occur. As a result, the reaction probability for a particular vibrational mode (*v*) is proportional to the overlap between the initial reactant vibrational wavefunction and the wavefunction at the transition state:

$$\Theta(v) \propto \left\langle \Psi_{CH_4}(v) \middle| \Psi_{TS} \right\rangle . \tag{13}$$

The Franck-Condon factor in the above equation reflects the limit that initial excited molecule do not have enough time to change when the molecule collides the surface, which is appropriate at large collision energies. Instead of computing the quantum overlap, we chose here to approximate the overlap using normal mode vectors. In this so called Sudden Vector Projection (SVP) model,[18] the overlaps between the normalized CH_4 normal mode vectors in the reactant asymptote and the normal mode vector corresponding to the imaginary frequency mode at the transition state are computed:

$$\left\langle \Psi_{CH_4}(v) \middle| \Psi_{TS} \right\rangle \approx \vec{Q}(v) \cdot \vec{Q}(s) . \tag{14}$$

The overlap in Eq. (14) was estimated from two geometries. The transition state geometry was take from the MEP analysis above. From this geometry, the distance between the CH_4 and the Ni surface was elongated along the Z coordinate towards the asymptote. With the non-reactive CH_3 group orientation fixed, the CH_4 moiety is optimized to recover at its equilibrium geometry. The resulting normal mode vectors in the reactant and transition state are used to evaluate the overlaps.

S-II. Additional results

A. Potential energy surface

To validate our slab model, the transition state (TS) for the dissociative chemisorption of CH_4 on Ni(111) was determined using the climbing-image nudged elastic band (CI-NEB) method.[19-20] The saddle point was verified by vibrational frequency analysis, which found a single imaginary frequency. The MEP from the initial state (IS) where the CH_4 is in gas phase to the final state (FS) where dissociation products CH_3 and H co-adsorbed in the nearest-neighbor positions was discretized by nine images, with the transition state as the highest image along the MEP. The convergence of the transition state energy is better than 0.02 eV with respect to both the plane wave basis cut off and the *k*-points.

As a first step, we optimized the structures for the IS, FS, and TS for the dissociative chemisorption of CH_4 on Ni(111) in full dimensionality with the parameters given in the main text. These stationary points and the minimum energy path obtained by the CI-NEB method are shown in Fig. 1 in the main text and Fig. S1, respectively. As extensively discussed in the literature, the cleaving C-H bond is significantly elongated at the transition state, forming a "late" barrier. The transition state is located at the top site and has a barrier height of 105.2 kJ/mol. Our results are consistent with previous DFT calculations on this system.[2-3,6,8,21]

To validate the accuracy of our PES, we first compare the properties of stationary geometries on the PES and those obtained by the plane wave DFT optimization, as shown in Table S1. The overall agreement is very good, for both the geometries and harmonic frequencies, although the latter are generally smaller than the experimental values[22] due to inherent errors in DFT. Most importantly, the fit reproduces the barrier height and imaginary frequencies at transition state. In addition, available data from the DFT calculations of Krishnamohan *et al.*[2] are also compared with our results in Table S1 and the stationary configurations and frequencies obtained from two calculations are very close to each other, indicating the adequacy of our DFT calculations. In Fig. S2, the MEP optimized in our PES is compared with and the MEP points computed directly by DFT. Again, the agreement is excellent and our potential captures the most important dynamic region for this reaction.

B. Wave packet calculations

To ascertain the convergence of the PES with respect to the number of points used in the fit, we have generated two additional PESs with 2,000 and 4,000 less points, respectively, randomly chosen from the data set. The resulting PESs yielded essentially the same reaction probabilities (data not shown). In addition, extensive tests have been performed with respect to the grid/basis sizes, the potential cutoff, and the propagation time to ensure convergence.

The vibrational frequencies of CH_4 were first determined within the 8D model and the results are listed in Table S2. It is clear that the frequencies of the symmetric stretching (v_1), asymmetric stretching (v_3), and umbrella (v_4) modes are reproduced quite accurately. However, the bending (v_2) mode frequency contains large errors. As discussed in our earlier work,[23] this error is due to the necessary departure from the C_{3v} symmetry in the CH_3 moiety during bending vibration. As a result, we will focus here on the v_1, v_3 and v_4 modes. In Fig. S3, the reaction probabilities calculated using the static surface model are displayed. It is clear that the mode selectivities are already apparent even without the site and lattice corrections discussed above.

C. Corrections of site and surface effects

Also included in Fig. S3 are the reaction probabilities with the surface mass model, where the Hamiltonian was modified. The changes are relatively minor. In Fig. S4, the effects of site averaging as well as the corrections concerning the electronic and mechanical couplings can be clearly seen. In particular, averaging over all possible impact sites in the unit cell decreases the reaction probability, due apparently to the increase of barrier height in impact sites other than the global transition state. In addition, as shown in the studies of Jackson and coworkers,[1,10] the surface lattice motion effects are substantial. Interestingly, the “electronic coupling”, which is introduced by sampling Q, significantly increases the reactivity in very low energy range, due apparently to the thermally induced puckering of the surface Ni atom which lowers the reaction barrier.[3,8] On the other hand, the "mechanical coupling" which is taken into account finally by averaging over *P*, decreases the reactivity at higher energies, in accord with "recoil effects" that present the energy transfer from impinging molecule to the lattice.[1] These corrections are critical to achieved a good agreement with the experimental data.

D. Vibrationally adiabatic model and non-adiabaticity

The calculated frequencies of the generalized normal modes are plotted in the upper panel of Fig. S5 as a function of the reaction coordinate (s) along the MEP. The vibrational state specific adiabatic potential energy curves are displayed in the lower panel of Fig. S5. The coupling of the *m*th generalized normal modes in the reaction path Hamiltonian with the reaction coordinate, namely B_{mF}, is collected in Table S3. As shown by the figure, the vibrational frequencies may undergo significant changes as the reaction progress. As a result, the vibrational state specific barriers may differ. As CH_4 approaches the surface, for example, the symmetric stretching mode "softens", reflected by the dramatic drop in its frequency near the transition state (s=0). This is due to the localization of the vibration in the cleaving C-H bond, indicative of its strong coupling with the reaction coordinate.[24] As a result, the corresponding barrier for this "reactive" mode (80.79 kJ/mol) is substantially lowered from that for the ground vibrational state (95.69 kJ/mol). Similarly, the umbrella bending also exhibits strong couplings with the reaction coordinate, evidenced by the drop of one of the three frequencies and the correspondingly lower reaction barrier (89.08 kJ/mol). The lowering of the barrier for the umbrella mode is less than the symmetric stretching mode, thus consistent with its smaller vibrational efficacy. As shown in Table S3, the symmetric stretching (v_1), bending (v_2), and umbrella (v_4) modes are strongly coupled with the reaction coordinate.

The asymmetric stretching mode, which also possesses significant enhancement, is a “spectator mode” in the vibrationally adiabatic model. The enhancement presumably stems from coupling to the reaction coordinate and intermodal couplings. As listed in Table S3, the coupling of the three asymmetric stretching modes with the reaction coordinate is quite small, but non-zero. As suggested by Jackson and Nave,[1] this coupling is capable of inducing significant enhancement by converting it vibrational energy to kinetic energy along the reaction coordinate. An alternative channel is via energy flow from the asymmetric stretching to symmetric stretching modes. As first noted by Halonen et al.[24] and later by Krishnamohan et al.,[2] there is an avoided crossing between the two vibrationally adiabatic potential curves in the entrance channel. The Massey velocity calculated at the avoided crossing near s = -4.305 amu$^{1/2}$bohr is 1.659×10^{-10} kg$^{1/2}$m/s, which is close to previously reported values.[2,24] If we consider the initial collision energy range that represents moderate reactivity in this work, which is from about 50 to100 kJ/mol, then add the ΔE_{vib} (0.62 kJ/mol) and minus V_{ac} (23.93 kJ/mol) at the avoid crossing according to Eq. (23), the corresponding collision velocities are thus ranging from 2.906×10^{-10} kg$^{1/2}$m/s to 4.662×10^{-10} kg$^{1/2}$m/s. As a result, the Massey parameters are from 0.356 to 0.571, which clearly indicate substantial vibrational non-adiabaticity. These vibrationally non-adiabatic transitions are likely responsible for the enhancement by exciting the asymmetric stretching mode of CH_4.

E. Sudden model

The calculated overlaps in the SVP model are summarized in Table S4, which predict the same trend observed in experiment and theory. While both the adiabatic and sudden models offer insights into the reaction dynamics and mode selectivity, it appears that the SVP model is closer to reality, given the large kinetic energy of the impinging molecule. These two models provide a complementary picture of the reaction dynamics.

Table S1. Comparison of the properties of stationary points on the PES and those obtained directly by the plane wave DFT optimization. The bond lengths are in Å, bond angle in degree, harmonic frequency in cm^{-1}, zero point energy and energy in kJ/mol. Previous data from Ref. [2] are also included for comparison while available.

Species	Properties	DFT	PES	Ref. [2]
CH$_4$ in gas phase	$r_{\text{C-H}}$	1.097	1.098	-
	$\theta_{\text{H-C-H}}$	109.5	109.3	-
	ω_1	3079	3048	3096
	ω_2	3078	3048	3085
	ω_3	3071	3048	3083
	ω_4	2965	2929	2978
	ω_5	1513	1496	1514
	ω_6	1504	1496	1514
	ω_7	1286	1279	1296
	ω_8	1285	1279	1294
	ω_9	1282	1278	1293
	ZPE	114.06	113.05	114.52
transition state 	$r_{\text{C-H1}}$	1.099	1.099	1.10
	$r_{\text{C-H2}}$	1.099	1.099	1.10
	$r_{\text{C-H3}}$(closest to H4)	1.099	1.100	1.10
	$\theta_{\text{H1-C-H2}}$	111.6	113.5	112
	$r_{\text{C-H4}}$(dissociating bond)	1.603	1.570	1.59
	Z_{C}	2.113	2.108	2.13
	$\theta_{\text{Ni-C-H4}}$	48.1	48.2	48
	$\theta_{\text{H3-C-H4}}$	80.0	79.9	80
	ω_1	3048	3126	3066
	ω_2	3033	3091	3048
	ω_3	2941	2951	2953
	ω_4	1599	1659	1556
	ω_5	1390	1435	1394
	ω_6	1354	1394	1347
	ω_7	1135	1160	1126
	ω_8	763	773	755
	ω_9	679	700	678
	ω_{10}	359	406	390
	ω_{11}	288	122	352
	ω_i	$959i$	$1017i$	$890i$
	ZPE	99.24	100.54	99.66
	Barrier	105.17	106.61	105.17

Table S2. Comparison of the CH_4 vibrational energies obtained from the 8D model and the experimental values.

Vibrational states (v_1,v_2,v_3,v_4)	Calc. (cm^{-1})	Expt. (cm^{-1})[a]
(0,0,0,1)	1259	1306
(0,0,1,0)	2499	1533
(1,0,0,0)	2889	2916
(0,0,1,0)	2939	3019

[a] Ref. [22]

Table S3. Maximum $B_{m\mathrm{F}}$ (coupling between generalized normal mode *m* and the reaction coordinate F) in the entrance channel (s<0).

Vibration	Mode *m*	Max ($b_{m\mathrm{F}}$)	Position *s* (amu$^{1/2}$•bohr)
Asymmetric stretch	1	0.133	-0.011
	2	0.084	-0.763
	3	0.143	-0.011
Symmetric stretch	4	-2.026	-0.760
Bending	5	-2.564	-0.695
	6	-2.457	-0.680
Umbrella Bending	7	-2.167	-0.643
	8	1.840	-0.593
	9	0.792	-0.454

Table S4. Overlaps between the CH_4 normal mode vectors at initial state with the vector corresponding to the reaction coordinate at transition state on the DFT PES.

Vibration	Mode *m*	Frequency (cm^{-1})	Overlap	Averaged overlap
Asymmetric stretch	1	3048	0.034	0.314
	2	3048	0.345	
	3	3048	0.562	
Symmetric stretch	4	2929	0.396	0.396
Bending	5	1496	0.057	0.238
	6	1496	0.419	
Umbrella Bending	7	1279	0.117	0.204
	8	1279	0.315	
	9	1278	0.182	

Fig. S1. Minimum energy path for the dissociative chemisorption of CH_4 on Ni(111) obtained by full-dimensional optimization.

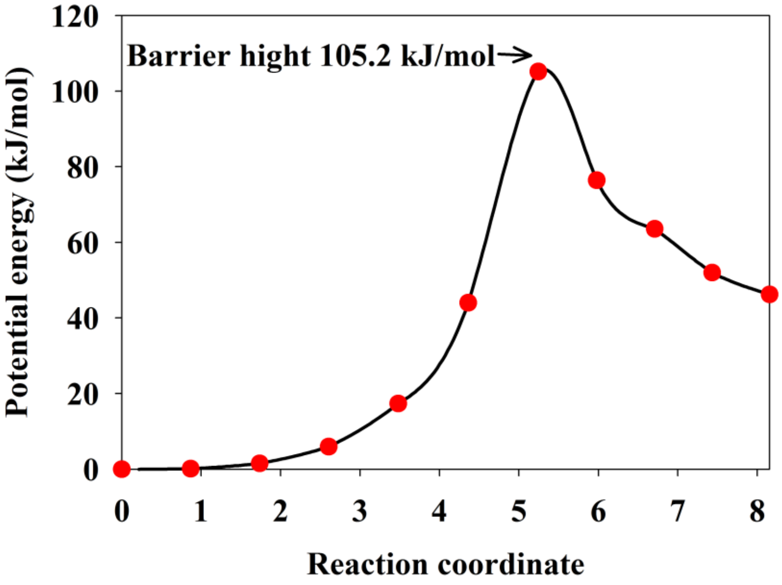

Fig. S2. Comparison between the MEP points and PES in our 12D model, where the energies are related to asymptotic CH_4+Ni .

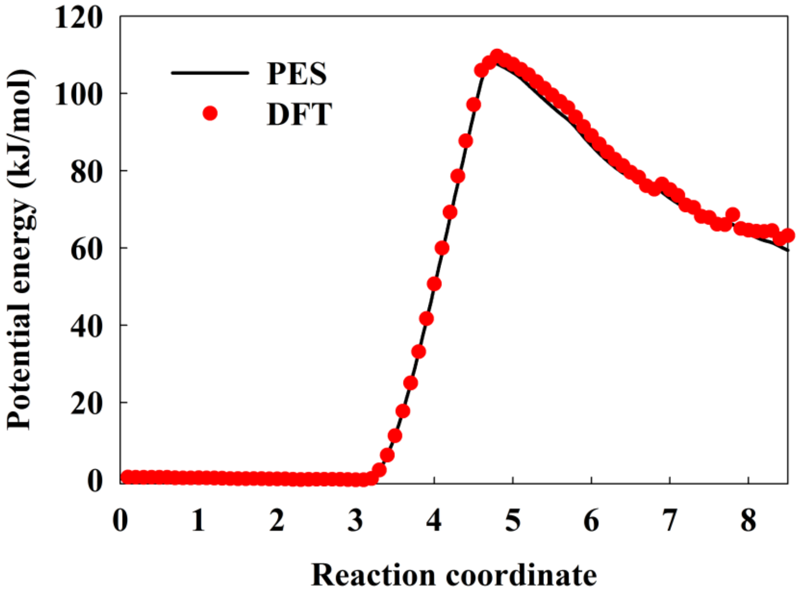

Fig. S3. Calculated total reaction probabilities as a function of the collision energy for several CH_4 vibrational states obtained with the static surface (SS) model and the surface mass (SM) model.

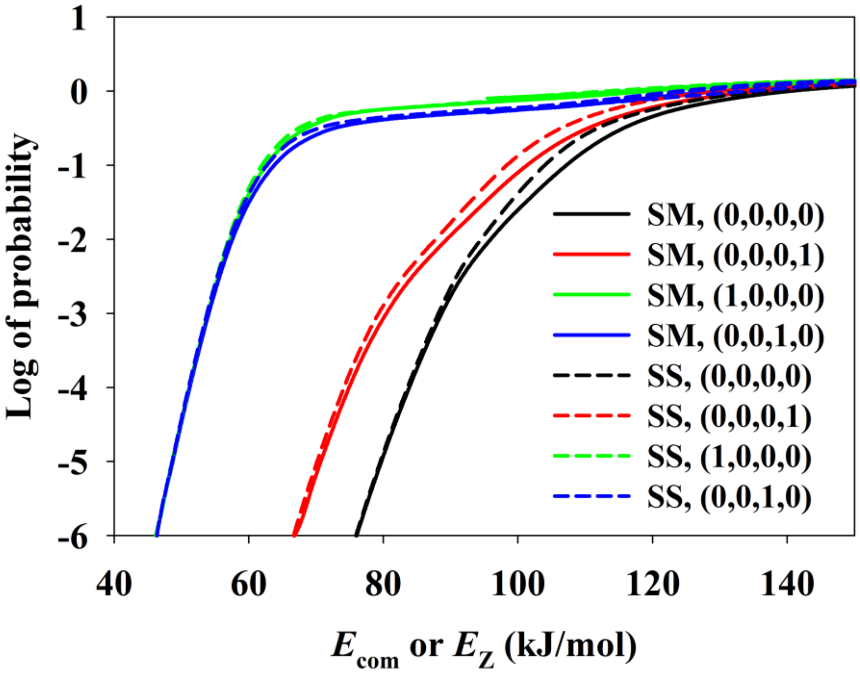

Fig. S4. Effects of various corrections with respect to the site, electronic and mechanical couplings on the reaction probability for the ground vibrational state of CH_4.

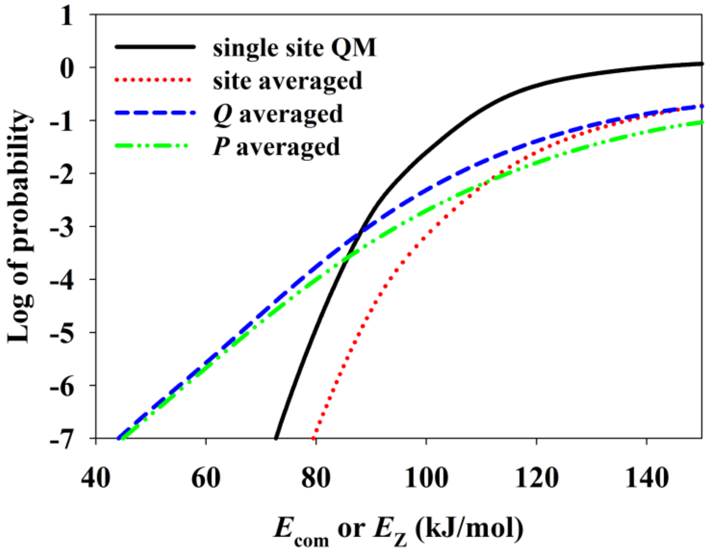

Fig. S5. Upper panel: frequencies of generalized normal modes along the reaction coordinate (*s*). The 1, 2, 3 modes correspond to the asymmetric stretching (as, v_3) modes of CH_4, 4 to the symmetric stretching (ss, v_1) mode, 5 and 6 to the bending (b, v_2) modes, and 7, 8, 9 to the umbrella (u, v_4) mode. Lower panel: adiabatic potential curves along the reaction coordinate (*s*) for the ground and vibrationally excited states of CH_4.

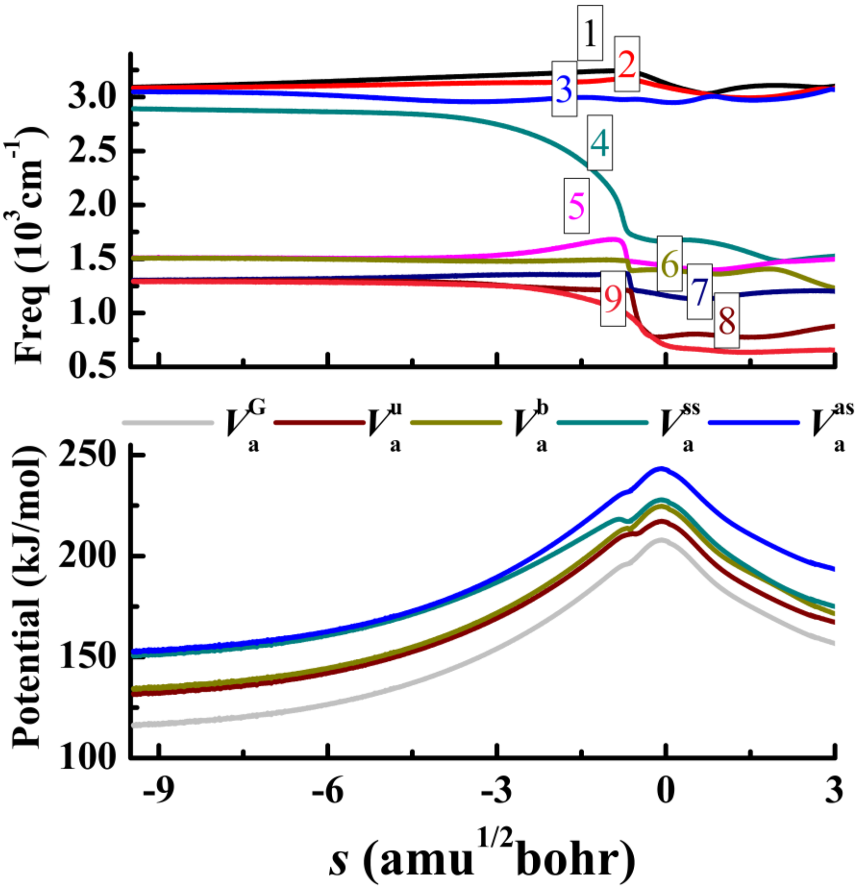

References:

(1) Jackson, B.; Nave, S. *J. Chem. Phys.* **2011**, *135*, 114701.

(2) Krishnamohan, G. P.; Olsen, R. A.; Valdes, A.; Kroes, G.-J. *Phys. Chem. Chem. Phys.* **2010**, *12*, 7654.

(3) Nave, S.; Jackson, B. *J. Chem. Phys.* **2009**, *130*, 054701.

(4) Dai, J.; Light, J. C. *J. Chem. Phys.* **1997**, *107*, 1676.

(5) Bengaard, H. S.; Nørskov, J. K.; Sehested, J.; Clausen, B. S.; Nielsen, L. P.; Molenbroek, A. M.; Rostrup-Nielsen, J. R. *J. Catal.* **2002**, *209*, 365.

(6) Henkelman, G.; Arnaldsson, A.; Jónsson, H. *J. Chem. Phys.* **2006**, *124*, 044706.

(7) Nave, S.; Jackson, B. *Phys. Rev. Lett.* **2007**, *98*, 173003.

(8) Nave, S.; Jackson, B. *J. Chem. Phys.* **2007**, *127*, 224702.

(9) Tiwari, A. K.; Nave, S.; Jackson, B. *Phys. Rev. Lett.* **2009**, *103*, 253201.

(10) Tiwari, A. K.; Nave, S.; Jackson, B. *J. Chem. Phys.* **2010**, *132*, 134702.

(11) Luntz, A. C.; Harris, J. *Surf. Sci.* **1991**, *258*, 397.

(12) Miller, W. H.; Handy, N. C.; Adams, J. E. *J. Chem. Phys.* **1980**, *72*, 99.

(13) Corchado, J. C.; Chuang, Y.-Y.; Fast, P. L.; Hu, W.-P.; Liu, Y.-P.; Lynch, G. C.; Nguyen, K. A.; Jackels, C. F.; Fernandez Ramos, A.; Ellingson, B. A.; Lynch, B. J.; Zheng, J.; Melissas, V. S.; Villà, J.; Rossi, I.; Coitiño, E. L.; Pu, J.; Albu, T. V.; Steckler, R.; Garrett, B. C.; Isaacson, A. D.; Truhlar, D. G.; University of Minnesota, Minneapolis: 2007.

(14) Page, M.; McIver, J. W. *J. Chem. Phys.* **1988**, *88*, 922.

(15) Jackels, C. F.; Gu, Z.; Truhlar, D. G. *J. Chem. Phys.* **1995**, *102*, 3188.

(16) Chuang, Y.-Y.; Truhlar, D. G. *J. Phys. Chem. A* **1998**, *102*, 242.

(17) Child, M. S. *Molecular Collision Theory*; Academic Press: London, 1974.

(18) Jiang, B.; Guo, H. *J. Chem. Phys* **2013**, *submitted*.

(19) Jónsson, H.; Mills, G.; Jacobsen, K. W. In *Classical and Quantum Dynamics in Condensed Phase Simulations*; Berne, B. J., Ciccotti, G., Coker, D. F., Eds.; World Scientific: Singapore, 1998.

(20) Henkelman, G.; Uberuaga, B. P.; Jónsson, H. *J. Chem. Phys.* **2000**, *113*, 9901.

(21) Kratzer, P.; Hammer, B.; Nørskov, J. K. *J. Chem. Phys.* **1996**, *105*, 5595.

(22) Herzberg, G. *Molecular Spectra and Molecular Structure, Vol. 3, Electronic Spectra of Polyatomic Molecules*; Van Nostrand: Princeton, 1966.

(23) Liu, R.; Yang, M.; Czakó, G.; Bowman, C. T.; Li, J.; Guo, H. *J. Phys. Chem. Lett.* **2012**, *3*, 3776.

(24) Halonen, L.; Bernasek, S. L.; Nesbitt, D. J. *J. Chem. Phys.* **2001**, *115*, 5611.